CSIRO PUBLISHING

Australian Journal of Physics

Volume 53, 2000
© CSIRO Australia 2000

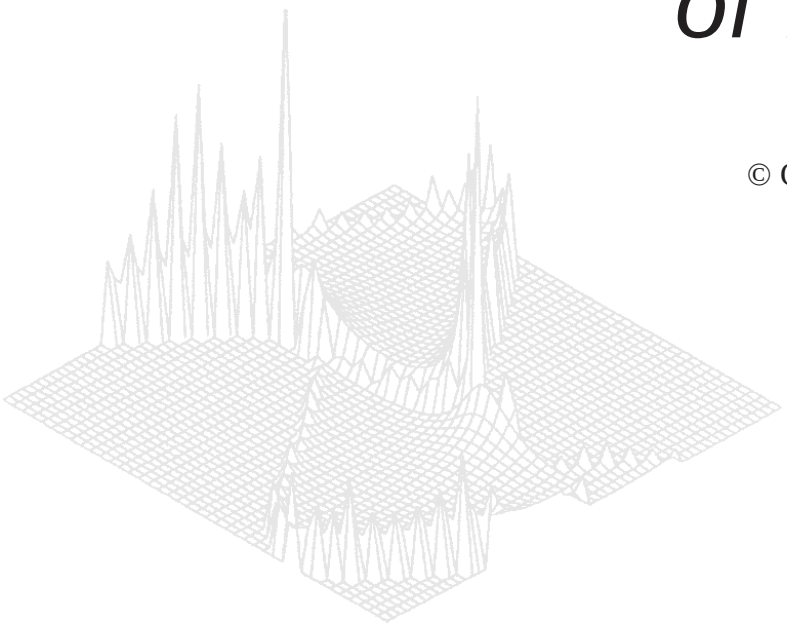

A journal for the publication of
original research in all branches of physics

www.publish.csiro.au/journals/ajp

All enquiries and manuscripts should be directed to
Australian Journal of Physics
CSIRO PUBLISHING
PO Box 1139 (150 Oxford St)
Collingwood Telephone: 61 3 9662 7626
Vic. 3066 Facsimile: 61 3 9662 7611
Australia Email: peter.robertson@publish.csiro.au

Published by **CSIRO** PUBLISHING
for CSIRO Australia and
the Australian Academy of Science

Aust. J. Phys., 2000, **53**, 87–105

Dynamical Properties of a Terahertz Driven Two-dimensional Electron Gas*

W. Xu

Department of Engineering Physics,
Institute for Superconducting and Electronic Materials,
University of Wollongong, Wollongong, NSW 2522, Australia.
wxu@wumpus.its.uow.edu.au

Abstract

In this paper, I present a detailed theoretical study on how a nanostructure, such as a semiconductor-based two-dimensional electron gas (2DEG), interacts with a linearly polarised intense laser field. A tractable method in dealing with the time-dependent many-body problem has been developed, from which the electron Green's function, the electron density–density correlation function and the inverse dielectric function matrix for a 2DEG driven by intense laser fields have been obtained. Using these results, the influence of terahertz laser radiation on dynamical properties such as plasmon and optical spectra in a 2DEG is investigated. The results obtained from this study can be used for the case where the intense terahertz radiation is provided by recently developed free-electron laser sources.

1. Introduction

In recent years, there has been a rapid expansion worldwide in developing high-power, tunable and long- and short-wavelength laser sources such as free-electron lasers (FELs). The FELs are generated by passing an intense beam of relativistic electrons through periodic magnetic fields and can provide linearly polarised laser radiation. In the long-wavelength regime, the current generation of the FELs† has already been able to provide a tunable source of a linearly polarised intense laser field in terahertz (10^{12} Hz or THz) or far-infrared (FIR) bandwidths. In the short-wavelength regime, people are working on X-ray FELs which will become the fourth generation of synchrotron radiation. At present, an extensive effort in building up more powerful, more compact and much cheaper FEL sources is underway internationally.

More importantly, since 1995 (Asmar *et al.* 1995) the THz FEL radiations have been successfully applied in scientific research into optoelectronic properties in novel condensed matter materials, such as low-dimensional semiconductor systems (LDSS) and semiconductor nanostructures (SNS). This has opened up an entirely new field of research in condensed matter physics and semiconductor optoelectronics. From a fundamental point of view, for GaAs- and Si-based

* Refereed paper based on a talk presented to the Workshop on Nanostructures and Quantum Confinements, held at the Australian National University, Canberra, in December 1998.
† The information about recent developments in free-electron lasers can be obtained from http://sbfe13.ucsb.edu/www/vl_fd.html.

© CSIRO 2000 10.1071/PH99041 0004-9506/00/010087$10.00

LDSS in which the conducting electrons are confined within nanometre distances, so that the electron kinetic energy and the electronic subband energy are of the order of meV, '*terahertz*' is a very interesting and under-explored frequency range lying between 'optical' and 'electrical' phenomena. When a low-dimensional electron gas (LDEG), as realised in, e.g. a LDSS, is subjected to an intense THz laser field (noting that a THz frequency, $\omega \sim$ THz, corresponds to an meV energy, $\hbar\omega \sim$ meV), we enter a regime of different competing energies where the electron kinetic energy, the electronic subband separation and the Fermi, phonon and plasmon energies can be comparable to the THz photon energy and to that of the radiation field. As a result, the THz laser field can couple strongly to the LDSS. Moreover, it has been realised that in an LDSS, the rate of electron–phonon and electron-impurity scattering can also be comparable to the frequency of the THz laser field (Xu and Zhang 1996). This implies that THz laser radiation will modify strongly the processes of momentum and energy relaxation for excited electrons in the system. These features allow us to observe and study photon-induced novel quantum effects and, by using these effects, to design and develop novel electronic and optoelectronic devices. Currently, an Australian research team from the University of Wollongong is working on the interactions between LDSS and THz FEL radiation (Koenraad *et al.* 1998), by using the so-called FELIX free-electron lasers (Free Electron Laser for Infrared eXperiment, from the FOM Institute for Plasma Physics, The Netherlands).

The fundamentally new experimental observations such as THz resonant-absorption (Asmar *et al.* 1995), THz photon-modified high-field magnetotransport (Koenraad *et al.* 1998), the THz photon-enhanced hot-electron effect (Asmar *et al.* 1996), the dynamical Franz–Keldysh effect (Nordstrom *et al.* 1998; Johnsen and Jauho 1998), THz photon-induced impact ionisation (Markelz *et al.* 1996), to mention but a few, indicate strongly that the field of LDSS interactions with intense THz laser radiation is very rich in terms of physics and in device applications. An understanding of these important experimental findings depends heavily on a sophisticated knowledge of many aspects of the optoelectronic properties in LDSS in the presence of an intense laser field. To my knowledge, for these problems no simple and complete theory is available in the literature. The present study aims mainly at developing fundamental new approaches to the theory of electron interactions with intense laser fields in an LDSS. In this paper, I will limit myself to the case where a semiconductor-based two-dimensional electron gas (2DEG) (e.g. a heterojunction or a quantum well structure) is taken into consideration. In Sections 2 and 3 I derive the electron Green's function, the electron density-of-states, the electron density–density correlation function and the dynamical dielectric function matrix for a 2DEG driven by a linearly polarised electromagnetic (EM) radiation field. Then, in Sections 4 and 5, I investigate the influence of the frequency and intensity of the THz radiation on plasmon modes and the optical spectrum of a THz-driven 2DEG. In Section 6 further remarks on the theories developed in the present study are made, and our study is summarised.

2. Green's Function and Density-of-State

In this study I consider the situation where the growth direction of a 2DEG is along the z-axis (i.e. the 2DEG is formed along the xy plane) and an EM

field $A(t)$ is applied and polarised linearly along the 2D plane (taken along the x-axis and so $\mathbf{A}(t) = [A_0 \sin(\omega t), 0, 0]$). Here ω is the frequency of the EM field and the usual dipole approximation for the radiation field has been employed. In this configuration, the radiation field will not couple directly to the confining potential of the 2DEG. Hence, the linearly polarised EM field plays the role of a driving field and that is why the combination is called 'THz-driven 2DEG'. The single-electron Hamiltonian to describe this electron–photon system can be written as

$$H_0(t) = \frac{[p_x - eA(t)]^2 + p_y^2 + p_z^2}{2m^*} + U(z)\,. \tag{1a}$$

Here a parabolic-conduction-band structure has been considered, $p_x = -i\hbar\partial/\partial x$ is the momentum operator, $A(t)$ is the vector potential induced by the EM field polarised along the x-direction, m^* is the effective electron mass, and $U(z)$ is the confinement potential energy of the 2DEG. Furthermore, I have used the Coulomb gauge (Shankar 1980) to describe the EM field. The usage of this gauge allows us to choose the vector potential $\mathbf{A}(t)$ and the scalar potential $\phi(t)$ for the radiation field such that $\nabla \cdot \mathbf{A}(t) = 0$ and $\phi(t) = 0$. These gauge conditions correspond to the situation where the charge density $\rho = 0$ and the current density $\mathbf{j} = 0$, which is true for the case of free electrons in a 2DEG in the absence of scattering, inhomogeneity, external driving field, etc. The solution of the time-dependent Schrödinger equation

$$i\hbar\frac{\partial\Psi(\mathbf{R},t)}{\partial t} = H_0(t)\Psi(\mathbf{R},t) \tag{1b}$$

is obtained as

$$\Psi_{n,\mathbf{k}} = \Psi_{n,\mathbf{k}}(\mathbf{R},0)e^{-i[E_n(\mathbf{k})+E_{em}]t/\hbar}e^{ir_0k_x[1-\cos(\omega t)]}e^{i\gamma\sin(2\omega t)}\,, \tag{2a}$$

where

$$\Psi_{n,\mathbf{k}}(\mathbf{R},0) = e^{\mathbf{k}\cdot\mathbf{r}}\psi_n(z)\,. \tag{2b}$$

Here $\mathbf{R} = (\mathbf{r}, z) = (x, y, z)$, $\mathbf{k} = (k_x, k_y)$ is the electron wavevector along the 2D plane, n is the index for the nth electronic subband, and $E_n(\mathbf{k}) = \hbar^2k^2/2m^* + \varepsilon_n$ is the energy spectrum of the 2DEG with ε_n being the energy of the nth electronic subband. Furthermore, we have $r_0 = eF_0/m^*\omega^2$ with the dimension of length, with $F_0 = A_0\omega$ being the strength of the radiation electric field, $\gamma = (eF_0)^2/8m^*\hbar\omega^3$ which is dimensionless, and $E_{em} = 2\gamma\hbar\omega$ is the energy of the radiation field induced by the dynamical Franz–Keldysh effect (Nordstrom *et al.* 1998; Johnsen and Jauho 1998). Because the radiation field is polarised along the 2D plane, the Schrödinger equation along the growth direction is time-independent and $\psi_n(z)$ and ε_n in equation (2) are determined by

$$\left[-\frac{\hbar^2}{2m^*}\frac{\partial^2}{\partial z^2} + U(z) - \varepsilon_n\right]\psi_n(z) = 0\,. \tag{3}$$

From the time-dependent electron wavefunction given by equation (2), we can determine the retarded (+) and advanced (−) Green's functions for free electrons in the $(n, \mathbf{k}; t)$ representation (i.e. in t-space or time-representation) using time-dependent condensed matter theory (Mattuck 1976), which are obtained respectively as

$$G^{+}(n, \mathbf{k}; t > t') = -\frac{i}{\hbar}\Theta(t - t')U(n, \mathbf{k}; t, t')\,, \tag{4a}$$

$$G^{-}(n, \mathbf{k}; t > t') = \frac{i}{\hbar}\Theta(t - t')U(n, \mathbf{k}; t', t)\,, \tag{4b}$$

where $\Theta(x)$ is the unit-step function and

$$U(n, \mathbf{k}; t, t') = e^{-i[E_n(\mathbf{k})+E_{em}](t-t')/\hbar} e^{-ir_0 k_x[\cos(\omega t)-\cos(\omega t')]} \times e^{i\gamma[\sin(2\omega t)-\sin(2\omega t')]} \tag{4c}$$

is the unitary operator which can be used to derive e.g. the electronic transition rate for electron–photon–phonon scattering (Xu 1998). Here the retarded Green's function satisfies

$$\left[i\hbar\frac{\partial}{\partial t} - \frac{[\hbar\mathbf{k} - e\mathbf{A}(t)]^2}{2m^*} - \varepsilon_n\right] G^{+}(n, \mathbf{k}; t > t') = \delta(t - t')\,. \tag{5}$$

With the electron Green's function in t-space, we can determine the Green's function in the $(n, \mathbf{k}; \Omega)$ representation (i.e. in Ω-space or the spectrum-representation). For example, the steady-state retarded Green's function for a 2DEG driven by an EM field in Ω-space can be obtained from (1) Fourier analysing $G^{+}(n, \mathbf{k}; t > t')$ according to time relative-coordinates $\tau = t - t'$ and (2) averaging the initial time t' over a period of the EM field, which reads

$$G^{+}_{n,\mathbf{k}}(E) = \sum_{M=-\infty}^{\infty} \frac{F_M^2(k_x)}{E - E_n(\mathbf{k}) - E_{em} - M\hbar\omega + i\delta}\,, \tag{6a}$$

where $E = \hbar\Omega$ is the electron energy, $M > 0$ ($M < 0$) corresponds to channels for M-photon absorption (emission), $M = 0$ corresponds to a channel for elastic photon scattering, and

$$F_M(k_x) = \sum_{N=-\infty}^{\infty} J_N(\gamma) J_{2N-M}(r_0 k_x) \tag{6b}$$

with $J_N(x)$ being a Bessel function.

From the imaginary part of the retarded electron Green's function in Ω-space, we can immediately obtain the electron density-of-state (DoS). The steady-state DoS for a 2DEG driven by an EM field is given by

$$D_n(E) = D_0 \sum_{M=-\infty}^{\infty} \Theta(\mathcal{E}_{Mn}) R_M(\mathcal{E}_{Mn})\,. \tag{7a}$$

Here $D_0 = m^*/\pi\hbar^2$, $\mathcal{E}_{Mn} = E - \varepsilon_n - E_{em} - M\hbar\omega$, and

$$R_M(x) = \frac{2}{\pi}\int_0^1 \frac{dy}{\sqrt{1-y^2}}\; F_M^2\left(y\sqrt{Fr2m^*x\hbar^2}\right). \tag{7b}$$

At high-frequency ($\omega \gg 1$) and/or for low-intensity ($F_0 \ll 1$) radiation, equation (7) becomes

$$D_n(E) = D_0\Theta(E - \varepsilon_n)\,, \tag{8}$$

which is the well-known result obtained for the DoS of a 2DEG in the absence of the radiation field.

The electron DoS is one of the central quantities to determine and to understand almost all physically measurable properties. In the presence of intense EM radiation, electrons in a 2DEG system can interact with the radiation field via channels for optical absorption ($M > 0$) and emission ($M < 0$) and for elastic optical process ($M = 0$). Therefore, now the electron DoS comes from all possible optical processes (see equation 7) and a factor $F_M^2(k_x)$ plays a role in switching different optical channels (see equation 6). The contribution from different optical processes to the electron DoS in a GaAs-based 2DEG (for GaAs $m^* = 0{\cdot}0665m_e$ with m_e being the rest electron mass) is shown in Fig. 1 at a fixed radiation field with a frequency ω and an intensity F_0. In the low electron energy regime, the electron DoS is induced mainly by the processes of optical emission. Noting that for an electron gas system the lower energy regime is more possibly occupied by electrons, the optical emission, including multiphoton processes, will play an important role in determining the electronic, optical and optoelectronic properties of a THz-driven 2DEG. In the high electron energy regime, the contribution to the electron DoS from optical absorption becomes more important. When the channel for elastic optical scattering opens up, a step increase in the DoS can be observed.

In the presence of the radiation field, the electron DoS will be shifted to the higher-energy regime (see equation 7) due to the dynamical Franz–Keldysh effect (DFKE). In Fig. 2, the electron DoS as a function of electron energy is shown at a fixed radiation frequency for different radiation intensities. Here $F_0 = 0$ corresponds to the case in the absence of the radiation field, for which the electron DoS of a 2DEG is characterised by a step-function (see equation 8). With increasing radiation intensity F_0, the energy of the radiation field $E_{em} = (eF_0)^2/4m^*\omega^2$, induced by DFKE, increases. As a result, with increasing F_0 the maximum electron DoS, induced by opening up of the elastic optical process, will be shifted to the higher-energy regime by a factor of E_{em}. For a GaAs-based 2DEG subjected to a THz laser field with $\omega/2\pi \sim 1$ THz and $F_0 \sim 10$ kV cm^{-1}, we have $E_{em} \sim 10$ meV. Very recently, the blue-shift of the electron DoS by E_{em} via DFKE has been successfully observed experimentally (Nordstrom *et al.* 1998) by applying THz FEL radiation to GaAs-based 2DEG systems. Furthermore, from Fig. 2 we see that in sharp contrast to the case in the absence of the EM radiation, the presence of the intense THz laser field will result in the DoS to be present in the low- and even negative-energy regime, due to the presence of the channels for optical emission.

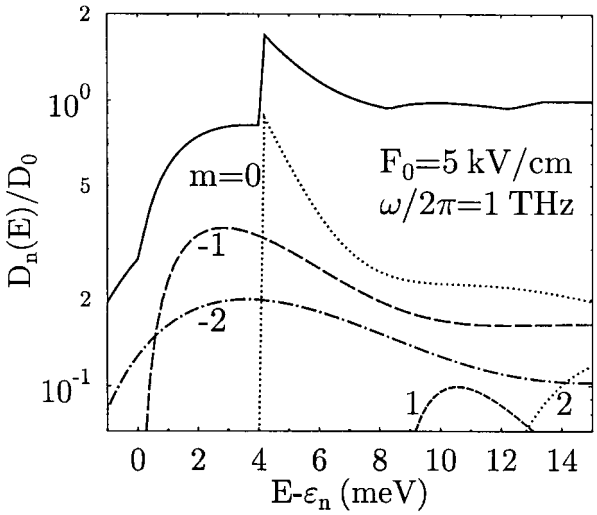

Fig. 1. The contribution from different optical processes to the electron density of states at a fixed radiation field with intensity F_0 and frequency ω. Here $m > 0$ and $m < 0$ correspond, respectively, to the channels of m-photon absorption and emission, while $m = 0$ corresponds to elastic optical scattering. When $F_0 = 5$ kV cm^{-1} and $\omega/2\pi = 1$ THz, we have $\hbar\omega \simeq 4{\cdot}14$ meV and $E_{em} = (eF_0)^2/4m^*\omega^2 \simeq 4{\cdot}19$ meV.

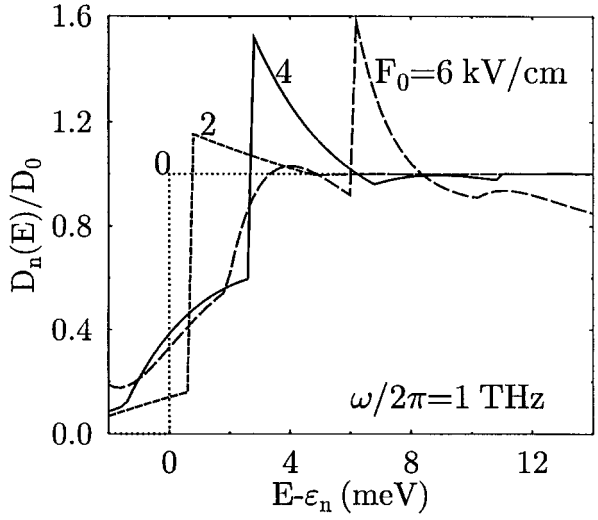

Fig. 2. Density of states for electrons in the nth subband as a function of electron energy E at a fixed radiation frequency for different radiation intensities F_0. Here ε_n is the electronic subband energy and $D_0 = g_s m^*/2\pi\hbar^2$.

A direct and important application of the electron DoS is to determine the Fermi energy in an electron gas system. Using the condition of electron number conservation, the Fermi energy E_F (or chemical potential) of a 2DEG system can be determined by

$$n_e = \sum_n \int_0^\infty dE \; f(E) D_n(E)\,, \tag{9}$$

where n_e is the electron density of the 2DEG and $f(E) = [e^{(E-E_F)/k_BT} + 1]^{-1}$ is the Fermi–Dirac function. By introducing the photon-modified electron DoS $D_n(E)$ (see equation 7) into equation (9), we can determine the photon-modified Fermi energy (see Fig. 4*a*).

3. RPA Inverse Dielectric Function Matrix

The dielectric response function measures the strength of an electron gas interacting via its long range force such as the Coulomb potential. Therefore, in modern condensed matter physics and electronics, the dielectric function plays an important role in discussing the many body problem and in studying elementary electronic excitations and the optical spectrum in an electron gas device.

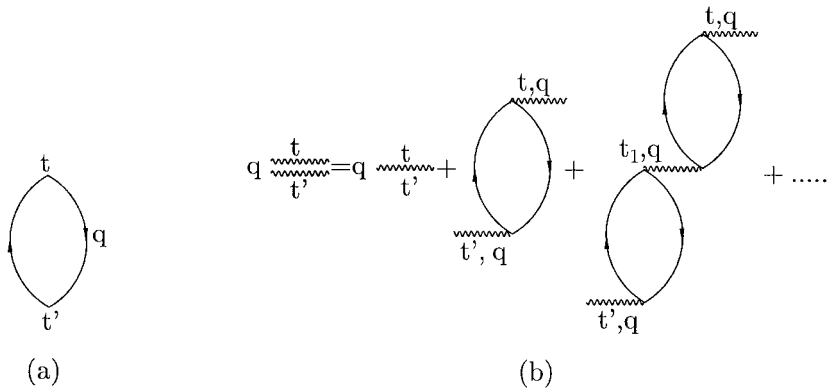

Fig. 3. Diagrams for an electron gas in time-representation: (*a*) the pair bubble or electron density–density correlation function and (*b*) the effective electron—electron interaction under the random-phase approximation.

For a Fermi system at finite temperatures, the pair bubble in t-space for a 2DEG is defined, in the absence of the electron-electron (e–e) interaction, by (see Fig. 3*a*)

$$-i\Pi_{n'n}(\mathbf{q};t,t') = -ig_s \sum_{\mathbf{k}} \frac{1}{\beta} \sum_{j=-\infty}^{\infty} [iG^-(n,\mathbf{k};t>t')e^{-i\omega_j(t-t')}] \times [iG^+(n',\mathbf{k}+\mathbf{q};t>t')e^{i\omega_j(t-t')}]\,, \tag{10a}$$

where $\beta = 1/k_BT$, $\omega_j = (2j+1)\pi/\beta$, $\mathbf{q} = (q_x, q_y)$, and $g_s = 2$ accounts for the spin degeneracy. Following the standard approach to evaluate the pair bubble (Mattuck 1976), the density–density (d–d) correlation function for a 2DEG in the $(n,\mathbf{k};t)$ representation is obtained as

$$\Pi_{n'n}(\mathbf{q};t,t') = g_s \frac{i}{\hbar}\Theta(t-t')e^{-ir_0q_x[\cos(\omega t)-\cos(\omega t')]} \sum_{\mathbf{k_1}} \Delta f_1 e^{-i\Delta E_1(t-t')/\hbar}\,. \tag{10b}$$

Here I have defined $\Delta f_j = f[E_n(\mathbf{k}_j) + 2\gamma\hbar\omega] - f[E_{n'}(\mathbf{k}_j + \mathbf{q}) + 2\gamma\hbar\omega]$, $f(x)$ is the Fermi–Dirac function, and $\Delta E_j = E_{n'}(\mathbf{k}_j + \mathbf{q}) - E_n(\mathbf{k}_j)$.

For a high-density electron gas system at low-temperatures, the random-phase approximation (RPA) can be used to study the effective e–e interaction. In t-space, the RPA diagrams for the e–e interaction are given by Fig. 3*b*. Moreover, in a quasi-2DEG system, the presence of the electronic subbands results in the fact that the system is in nonequilibrium. Therefore, the bare and effective e–e interactions are in the form of a matrix. Using the RPA diagrams given by Fig. 3*b*, the matrix element for the effective e–e interaction can be calculated through

$$\begin{aligned} -iV^{\text{eff}}_{\alpha\beta}(\mathbf{q};t,t') = {} & [-iV_{\alpha\beta}(q)]\delta_{\alpha,\beta}\delta(t-t') \\ & + [-iV_{\alpha\beta}(q)][-i\Pi_\beta(\mathbf{q};t,t')][-iV_{\alpha\beta}(q)] \\ & + \int_{t'}^{t} dt_1 \ [-iV_{\alpha\beta}(q)][-i\Pi_\beta(\mathbf{q};t_1,t')] \\ & \times [-iV_{\alpha\beta}(q)][-i\Pi_\beta(\mathbf{q};t,t_1)][-iV_{\alpha\beta}(q)] + ... \end{aligned} \tag{11}$$

Here $\alpha = (n'n)$ and $V_{\alpha\beta}(q)$ is the Fourier transform of the matrix element for the bare e–e interaction

$$V_{\alpha\beta}(q) = \frac{2\pi e^2}{\kappa q} \int dz_1 dz_2 \ f_\alpha(z_1) f_\beta(z_2) e^{-q|z_1 - z_2|} \,, \tag{12}$$

where κ is the dielectric constant of the material and $f_\alpha(z) = \psi^*_{n'}(z)\psi_n(z)$. Introducing the pair bubble obtained in t-space (equation 10b) into equation (11), the effective e–e interaction can be written in the form

$$[\mathbf{V^{eff}}] = [\mathbf{V}][\epsilon]^{-1} \,, \tag{13}$$

where $[\mathbf{V^{eff}}]$ and $[\mathbf{V}]$ are the matrices with, respectively, the elements $V^{eff}_{\alpha\beta}(\mathbf{q};t,t')$ and $V_{\alpha\beta}(q)$. Hence, by definition, $[\epsilon]^{-1}$ is the inverse dielectric function matrix for a 2DEG in the $(n,\mathbf{k};t)$ representation, namely

$$[\epsilon]^{-1} = e^{-ir_0 q_x[\cos(\omega t) - \cos(\omega t')]} \left[[\mathbf{I}]\delta(t-t') + \frac{i}{\hbar}\Theta(t-t') \sum_{j=1}^{\infty} (-g_s[\mathbf{V}])^j [\mathbf{R_j}] \right] . \tag{14}$$

In equation (14), $[\mathbf{I}]$ is the unitary matrix and the element of the matrix $[\mathbf{R_j}]$ is $R_j(\beta,\mathbf{q};t-t')$ where

$$R_1(n',n,\mathbf{q};\tau) = \sum_{k_1} \Delta f_1 e^{-i\Delta E_1 \tau/\hbar} \,; \tag{15a}$$

$$R_2(n',n,\mathbf{q};\tau) = \sum_{k_1,k_2} \Delta f_1 \Delta f_2 \left[\frac{e^{-i\Delta E_1\tau/\hbar}}{\Delta E_1 - \Delta E_2} + \frac{e^{-i\Delta E_2\tau/\hbar}}{\Delta E_2 - \Delta E_1} \right] ; \tag{15b}$$

and

$$R_j(n',n,\mathbf{q};\tau) = \sum_{k_1,k_2,\ldots,k_j} \Delta f_1 \Delta f_2 ... \Delta f_j \tag{15c}$$

$$\times \left[\frac{e^{-i\Delta E_1 \tau/\hbar}}{[\Delta E_1 - \Delta E_2]...[\Delta E_1 - \Delta E_j]} + ... + \frac{e^{-i\Delta E_j \tau/\hbar}}{[\Delta E_j - \Delta E_{j-1}]...[\Delta E_j - \Delta E_1]} \right].$$

The element of the inverse dielectric function matrix for a 2DEG in t-space is

$$\epsilon^{-1}_{\alpha\beta}(\mathbf{q};t,t') = e^{-ir_0 q_x[\cos(\omega t)-\cos(\omega t')]} \big[\delta_{\alpha,\beta}\delta(t-t') + \frac{i}{\hbar}\Theta(t-t') \sum_{j=1}^{\infty} [-g_s V_{\alpha\beta}(q)]^j R_j(\beta,\mathbf{q};t-t') \big] . \tag{16}$$

From the inverse dielectric function matrix in t-space, we can obtain the inverse dielectric function matrix in Ω-space by first Fourier analysing $\epsilon^{-1}_{\alpha\beta}(\mathbf{q};t,t')$ according to time relative-coordinates $\tau = t - t'$ and then averaging the initial time t' over a period of the radiation field. For a steady state, the inverse dielectric function matrix element for a 2DEG in Ω-space is obtained as

$$\epsilon^{-1}_{\alpha\beta}(\mathbf{q},\Omega) = \sum_{M=-\infty}^{\infty} J_M^2(r_0 q_x)[\delta_{\alpha,\beta} - V_{\alpha\beta}(q)\Pi^0_\beta(q,\Omega+M\omega)]^{-1} , \tag{17a}$$

and the inverse dielectric function matrix is given by

$$[\epsilon]^{-1} = \sum_{M=-\infty}^{\infty} J_M^2(r_0 q_x) \big[[\mathbf{I}] - [\mathbf{V}][\mathbf{\Pi^0}] \big]^{-1} . \tag{17b}$$

Here, again, the index M corresponds to different optical channels and, therefore, the inverse dielectric function is the summation over all possible optical processes. Furthermore,

$$\Pi^0_{n'n}(q,\Omega) = g_s \sum_{\mathbf{k}} \frac{f[E_n(\mathbf{k}) + E_{em}] - f[E_{n'}(\mathbf{k}+\mathbf{q}) + E_{em}]}{\hbar\Omega + E_n(\mathbf{k}) - E_{n'}(\mathbf{k}+\mathbf{q}) + i\delta} \tag{17c}$$

is the Fourier transform of the electron d–d correlation function. From equation (17), we see that the presence of the linearly polarised radiation field will lead to an anisotropic inverse dielectric function which depends on q_x, the change of the electron wavevector along the direction where the EM field is polarised. The physical reason behind this is that the linearly polarised EM field can break the symmetry of the sample geometry.

For high-frequency ($\omega \gg 1$) and low-intensity ($F_0 \ll 1$) radiation, so that $r_0 q_x \ll 1$ and $\gamma \ll 1$, the dielectric function matrix of a 2DEG becomes

$$[\epsilon] = [\mathbf{I}] - [\mathbf{V}][\mathbf{\Pi^0}] , \tag{18a}$$

and the matrix element is given by

$$\epsilon_{\alpha\beta}(q,\Omega) = \delta_{\alpha,\beta} - V_{\alpha\beta}(q)\Pi^0_\beta(q,\Omega)\,, \tag{18b}$$

which are the well-known results obtained in the absence of the EM radiation field.

4. Plasmon Modes

The inverse dielectric function matrix for a 2DEG in the $(n,\mathbf{k};\Omega)$ representation can be directly applied to the study of the influence of an intense laser field on collective excitations in a 2DEG system. For a 2DEG with only one electronic subband, after referring the energy from $\varepsilon_n = \varepsilon_{n'} = 0$, the dielectric function becomes

$$\epsilon(\mathbf{q},\Omega) = \frac{\prod_{M=-\infty}^{\infty}[1 - V_{0000}(q)\Pi^0_{00}(q,\Omega + M\omega)]}{\sum_{M=-\infty}^{\infty} J_M^2(r_0 q_x) \prod_{M'=-\infty, M'\neq M}^{\infty}[1 - V_{0000}(q)\Pi^0_{00}(q,\Omega + M'\omega)]}\,. \tag{19}$$

In this case the plasmon modes induced by the charge-density excitation can be determined theoretically by taking Re $\epsilon(\mathbf{q},\Omega) \to 0$. In the low-temperature $(T \to 0)$ and long-wavelength $(q \ll 1)$ limit, the plasmon frequency of a 2DEG driven by an EM radiation field is obtained simply as

$$\Omega_p = \omega_p \Theta(E_F - E_{em}) \sqrt{\frac{m^*(E_F - E_{em})}{\pi\hbar^2 n_e}}\,, \tag{20}$$

where $\omega_p = (2\pi e^2 n_e q/\kappa m^*)^{\frac{1}{2}}$ is the plasmon frequency of a 2DEG in the absence of the EM radiation. Here we see that in the low-temperature and long-wavelength limit, the effect of the radiation field on plasmon modes in a 2DEG is mainly achieved via photon-modified Fermi energy. Furthermore, equation (20) indicates that in the presence of the radiation field, the plasmon excitation can only be possible when the Fermi energy of the electronic system is above the energy of the radiation field caused by DFKE. Noting that $E_F > E_{em}$ implies the presence of the channels for elastic photon scattering and for optical absorption, $E_F > E_{em}$ makes it possible for electronic transitions from occupied states to empty states via absorption of photons and, thus, the plasmon excitation can be achieved in a 2DEG system. When $E_F < E_{em}$, only the channels for optical emission are present in the electronic system. In this case, it is less possible for electronic transitions from an occupied state (lower energy level) to an empty state (higher energy level) via emission of photons and, therefore, it is not possible to observe the plasmon excitation.

In the presence of the intense laser field, the Fermi energy E_F depends on the intensity F_0 and frequency ω of the radiation (see equation 9). As a result, the plasmon frequency Ω_p varies with F_0 and ω. In Fig. 4*a* the Fermi energy

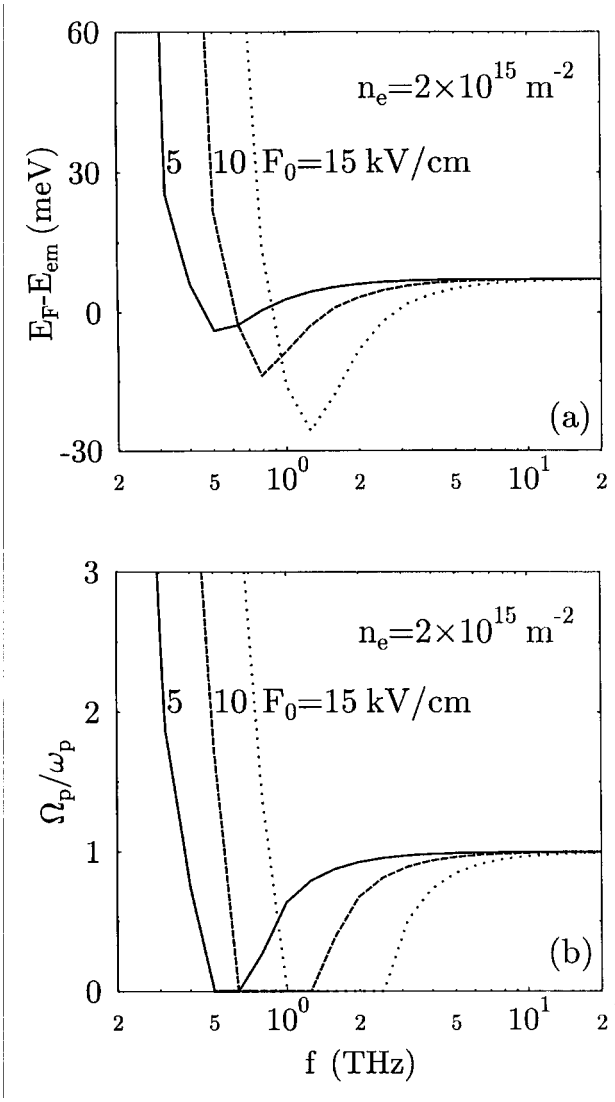

Fig. 4. (*a*) Fermi energy E_F measured from the energy of the radiation field, $E_{em} = (eF_0)^2/4m^*\omega^2$, as a function of the radiation frequency $f = \omega/2\pi$ for three values of the radiation intensity F_0 at a fixed electron density n_e. (*b*) Plasmon frequency Ω_p in units of the plasmon frequency ω_p in the absence of the laser field as a function of the radiation frequency $f = \omega/2\pi$, for the same values of F_0 and n_e as in part (*a*). The results are obtained for a GaAs-based one-subband 2DEG.

[measured from the energy of the radiation field] and in Fig. 4*b* the plasmon frequency [in units of the plasmon frequency in the absence of the radiation field] are plotted as a function of radiation frequency for different radiation intensities in a GaAs-based 2DEG system. As can be seen, in different radiation intensity and frequency regimes the Fermi energy and the plasmon frequency exhibit different features:

(1) Under low-frequency and/or high-intensity radiation, when the energy of the radiation field is much larger than the photon energy (i.e. $E_{em} \gg \hbar\omega$), E_F is determined mainly by E_{em} via the dynamical Franz–Keldysh effect. In this case, $E_F > E_{em}$, Ω_p increases with increasing F_0 and/or decreasing ω, and $\Omega_p > \omega_p$ can be observed.
(2) In an intermediate radiation intensity and frequency regime, E_F is determined mainly by photon emission processes, which results in $E_F < E_{em}$ and, therefore, the plasmon excitation is suppressed (i.e. $\Omega_p = 0$). This regime of ω and F_0 is a window for propagation of the EM wave in an electron gas system.
(3) For relatively high-frequency and/or low-intensity radiation, the Fermi energy is determined mainly by elastic optical processes and by processes of optical absorption so that $E_F > E_{em}$. In this case, Ω_p increases with increasing ω and/or decreasing F_0, and $\Omega_p < \omega_p$ can be observed.
(4) For high-frequency ($\omega \gg 1$) and/or low-intensity ($F_0 \ll 1$) radiation, entailing $r_0 \to 0$ and $\gamma \to 0$, the radiation field affects very weakly the Fermi energy and, consequently, the plasmon frequency Ω_p tends to that in the absence of the radiation ω_p.

These results indicate that by varying the frequency and/or intensity of the radiation field, a frequency tunable plasmon excitation can be achieved in a semiconductor-based 2DEG system.

5. Optical Spectrum

For a 2DEG system, because the plasmon frequency depends on the change of electron wavevector (i.e. $\omega_p \sim q^{\frac{1}{2}}$, see equation 20), it is much easier to measure experimentally the optical spectrum than to measure directly the plasmon modes. At present, optical studies have been popularly and widely used to measure the free electron density in inhomogeneous systems and to verify the dependence of the plasmon dispersion on electron density and wavevector in electronic systems (Voβebürger *et al.* 1996). Theoretically, the optical spectrum of an electron gas system can be obtained from the imaginary part of the inverse dielectric function, $E(\Omega) = \mathrm{Im}\epsilon^{-1}(\Omega)$, which measures the energy loss of fast electrons via absorption of the probing field with frequency Ω (Glicksman 1971). Here I consider the situation where a *deriving* EM field with frequency ω and intensity F_0 is linearly polarised along the 2D-plane of a 2DEG and a weak *probing* field with frequency Ω is applied to measure the optical spectrum. Moreover, in the present study, I limit myself to the situation where only one electronic subband is present in a 2DEG system. In this case, the inverse dielectric function of a 2DEG is given by

$$\frac{1}{\epsilon(\mathbf{q},\Omega)} = \sum_{M=-\infty}^{\infty} \frac{J_M^2(r_0 q_x)}{1 - V_{0000}(q)\Pi_{00}^0(q, \Omega + M\omega)}\,, \tag{21a}$$

with an imaginary part

$$\mathrm{Im}\frac{1}{\epsilon(\mathbf{q},\Omega)} =$$

$$\sum_{M=-\infty}^{\infty} \frac{J_M^2(r_0 q_x)\ V_{0000}(q)\ \mathrm{Im}\Pi_{00}^0(q,\Omega+M\omega)}{[1-V_{0000}(q)\ \mathrm{Re}\Pi_{0000}^0(q,\Omega+M\omega)]^2+[V_{0000}(q)\ \mathrm{Im}\Pi_{00}^0(q,\Omega+M\omega)]^2}\,. \tag{21b}$$

For studying a dynamical quantity such as the optical spectrum, Ω in equation (21) can be taken as the frequency of the probing field. The averaged imaginary part of the inverse dielectric function (or the so-called energy-loss function) is obtained as

$$E(\Omega) = \frac{1}{n_e}\sum_{\mathbf{q}} \mathrm{Im}\frac{1}{\epsilon(\mathbf{q},\Omega)} = \frac{1}{\pi}\int_0^{\pi} d\theta\ E(\Omega,\theta)\,, \tag{22a}$$

where θ is the polar angle to the x-axis along which the driving EM field is polarised and the angular distribution of the energy-loss function is

$$E(\Omega,\theta) = \sum_{M=-\infty}^{\infty} E_M(\Omega,\theta)\,, \tag{22b}$$

with the contribution from a M-photon process being

$$E_M(\Omega,\theta) =$$

$$\frac{1}{2\pi^2 n_e}\int_0^{\infty} \frac{dqq\ J_M^2(r_0 q\cos\theta)\ V_{0000}(q)\ \mathrm{Im}\Pi_{00}^0(q,\Omega+M\omega)}{[1-V_{0000}(q)\ \mathrm{Re}\Pi_{0000}^0(q,\Omega+M\omega)]^2+[V_{0000}(q)\ \mathrm{Im}\Pi_{00}^0(q,\Omega+M\omega)]^2}\,. \tag{22c}$$

In the presence of the linearly polarised driving EM field, the optical spectrum of an electron gas is anisotropic, i.e. it depends on the angle θ (see equation 22a). Equation (22b) reflects the fact that the optical spectrum now comes from all possible processes via electron interactions with the driving field. Furthermore, the change of the electron wavevector along the direction where the driving EM field is polarised (i.e. q_x) plays a role in switching different optical processes. For example, when $q_x \to 0$, only the 0-photon (i.e. elastic) process contributes to the optical spectrum. With increasing $|q_x|$, entailing $J_M(r_0 q_x) \neq 0$, other photon processes can contribute to the energy-loss function. For high-frequency $\omega \gg 1$ and/or low-intensity $F_0 \ll 1$ driving fields so that $r_0 \sim 0$ and $\gamma \sim 0$, the optical spectrum given by equation (22) becomes the well-known result obtained in the absence of the driving EM field and $\mathrm{Im}\epsilon^{-1}(\Omega,\theta) = \mathrm{Im}\epsilon^{-1}(\Omega)$ does not depend on the angle θ.

In the low-temperature limit (i.e. $T \to 0$) and taking $\varepsilon_0 = 0$, we have

$$\mathrm{Re}\Pi_{00}^0(q,\Omega) = -\Theta(E_F - E_{em})\frac{m^*}{2\pi\hbar^2\varepsilon_q}R(\varepsilon_q,\Omega)\,, \tag{23a}$$

$$\mathrm{Im}\Pi^0_{00}(q,\Omega) = -\Theta(E_F - E_{em})\frac{m^*}{2\pi\hbar^2\varepsilon_q} I(\varepsilon_q,\Omega)\,, \tag{23b}$$

where $\varepsilon_q = \hbar^2 q^2/2m^*$,

$$R(x,\Omega) = 2x - \mathrm{Re}\sqrt{(x-\hbar\Omega)^2 - 4x(E_F - E_{em})}$$

$$- \mathrm{Re}\sqrt{(x+\hbar\Omega)^2 - 4x(E_F - E_{em})}\,, \tag{23c}$$

$$I(x,\Omega) = \Theta(E_F - E_{em} - \hbar\Omega)\mathrm{Re}\sqrt{(a_+ - x)(x - a_-)}$$

$$- \Theta(E_F - E_{em} + \hbar\Omega)\mathrm{Re}\sqrt{(b_+ - x)(x - b_-)}\,, \tag{23d}$$

with

$$a_\pm = (\sqrt{E_F - E_{em}} \pm \sqrt{E_F - E_{em} - \hbar\Omega})^2\,,$$

$$b_\pm = (\sqrt{E_F - E_{em}} \pm \sqrt{E_F - E_{em} + \hbar\Omega})^2\,.$$

Equation (23) indicates that in the low-temperature limit, the optical spectrum of a 2DEG driven by an EM radiation field can only be observed when the Fermi energy of the system E_F is above the energy of the driving radiation field E_{em}. This can be understood by the fact that in the presence of the driving field, the dielectric response to the probing field, via electronic transitions accompanied by absorption of the probing and driving fields, can only occur when $E_F > E_{em}$. When $E_F < E_{em}$, the emission of photons by electrons will be the principal channel for relaxation of excited electrons in the system.

The results shown in Fig. 4*a* indicate that: (1) under low-frequency and/or high-intensity radiation, when $E_{em} \gg \hbar\omega$, we have $E_F > E_{em}$ and, therefore, the optical spectrum via dielectric response can be observed. (2) In an intermediate radiation frequency and intensity regime, E_F is determined mainly by photon emission processes and, consequently, $E_F < E_{em}$. In this case, the low-temperature optical spectrum via fast electron processes cannot be observed and this regime of F_0 and ω is a window for propagation of EM waves. (3) For relatively high-frequency and/or low-intensity radiation, when $E_{em} \sim \hbar\omega$, then E_F is determined mainly by 0-photon and photon absorption processes, and so $E_F > E_{em}$. In this case, $E_F - E_{em}$ increases with increasing ω and/or decreasing F_0 and the optical spectrum can be observed. (4) For $\omega \gg 1$ and/or $F_0 \ll 1$, entailing $E_{em} \to 0$ and $r_0 \to 0$, the radiation affects very weakly the Fermi energy and the optical spectrum tends to that observed in the absence of the laser field. Below I discuss the optical spectrum of an AlGaAs/GaAs heterojunction in the case of (3).

For GaAs the dielectric constant is $\kappa = 12 \cdot 9$. Here I make the usual triangular well approximation to model the confining potential normal to the interface of the heterojunction and use the corresponding variational wavefunction (Ando *et al.* 1982). In doing so, we have

$$V_{0000}(q) = \frac{2\pi e^2}{\kappa q} \frac{3y^2 + 9y + 8}{8(1+y)^3}\,, \tag{24}$$

where $y = q/b$ and $b = [(48\pi m^* e^2/\kappa\hbar^2)(N_{depl} + 11n_e/32)]^{\frac{1}{3}}$ defines the thickness of the triangular well with N_{depl} being the depletion charge density (typically $N_{depl} = 5 \times 10^{10}$ cm^{-2} for an AlGaAs/GaAs heterojunction).

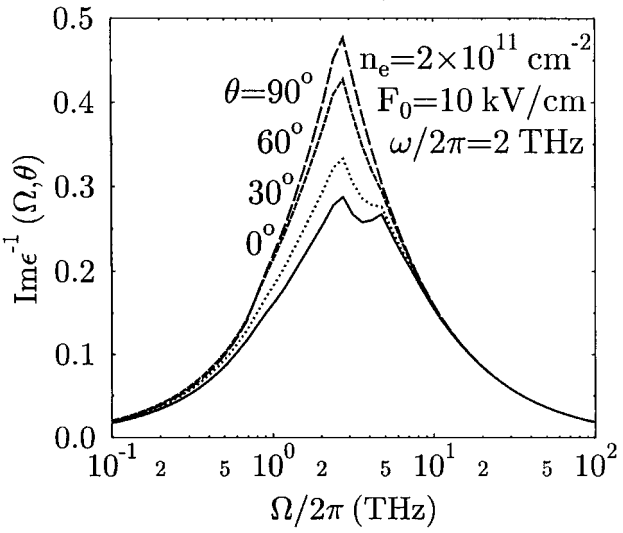

Fig. 5. Energy-loss function $E(\Omega, \theta) = \mathrm{Im}\epsilon^{-1}(\Omega, \theta)$ at a fixed driving field for different θ angles. Here θ is the polar angle to the x-axis along which the driving laser field is polarised and Ω is the frequency of the probing field.

The energy-loss function at a fixed driving field for different θ angles is shown in Fig. 5, where the angular dependence of the optical spectrum is evident. The variation of θ corresponds to the change of the possibility for electronic transitions achieved by change of the electron wavevector (or momentum) along the direction where the driving field is polarised. The variation of q_x will result in different processes of photon emission and absorption by electron interactions with the driving field. Therefore, the optical spectrum induced by dielectric response in the presence of an intense driving EM field depends on the angle θ. The case $\theta = 90°$ implies $q_x = 0$ and so only the zero-photon process gives rise to the energy-loss function. The case $\theta = 0$ corresponds to $q_x = q$ where the strongest effect of the driving field can be measured. The results obtained from further numerical calculations show that a stronger anisotropic feature of the optical spectrum can be observed at a driving field with higher radiation intensity and/or lower radiation frequency, because $r_0 = eF_0/m^*\omega^2$ (see equation 22).

The contribution to the energy-loss function from different optical processes due to electron interactions with the driving field is shown in Fig. 6 at a fixed driving field and at $\theta = 0$. In the presence of an intense driving EM field, the electronic transitions can be achieved by emission ($m < 0$) and absorption ($m > 0$) of photons, including multiphoton ($|m| > 1$) processes. These electronic

transition events can be observed by measuring the optical spectrum via dielectric response, as can be seen in Fig. 6. From Fig. 6, we note that for low-frequency probing fields, the energy-loss function caused by photon emission processes is negative, which implies an optical gain due to the interaction between electrons and the driving field. The results obtained from further calculations indicate that with increasing F_0 and/or decreasing ω of the driving field, a stronger effect of photon emission can be observed in the optical spectrum.

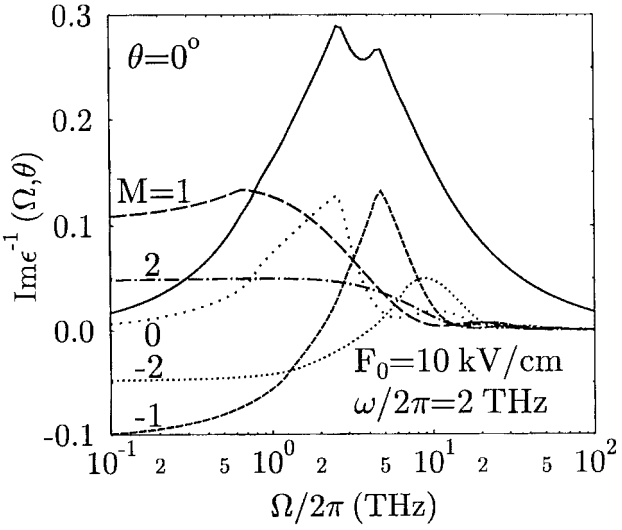

Fig. 6. Contribution from different optical processes to the optical spectrum at $\theta = 0^o$ for a fixed driving field. Here $M > 0$, $M < 0$ and $M = 0$ correspond, respectively, to the processes of photon absorption, emission and elastic photon scattering by electron interactions with the driving field. The solid curve is the total optical spectrum.

Fig. 7 shows the energy-loss function at a fixed ω and at $\theta = 0$ for different intensities of the driving field. With increasing F_0, the energy-loss function decreases. This is due to the following two reasons. (1) At $\omega/2\pi = 2$ THz and when $F_0 \leq 10$ kV cm^{-1}, $E_F - E_{em}$ decreases with increasing F_0 (see Fig. 4*a*). A smaller $E_F - E_{em}$ implies less channels for dielectric response accompanied by absorption of the driving and probing fields. (2) With increasing F_0, the electronic transitions via photon emission increase, which makes a negative contribution to the energy-loss function in some probing field regimes.

6. Further Notes and Summary

In this study, I have proposed and developed a tractable method in dealing with electron interactions with an intense laser field in a nanostructure such as a semiconductor-based 2DEG system. The theoretical approaches are based on the solution of the time-dependent Schrödinger equation in which the effect of the linearly polarised EM field is included.

(1) From the time-dependent electron wavefunction obtained from the solution of the time-dependent Schrödinger equation, I have derived the retarded

and advanced electron Green's functions in the time and spectrum representation.

(2) From the imaginary part of the retarded electron Green's function in the spectrum representation, I have determined the electron density of states.
(3) Using retarded and advanced electron Green's functions in the time representation, I have obtained the electron density–density correlation function (or pair bubble) for a Fermi system at finite temperatures in the time representation.
(4) Applying the electron density–density correlation function obtained to the random-phase approximation diagrams for the effective electron–electron interaction, I have obtained the inverse RPA dielectric function matrix in the time and spectrum representation.
(5) Using the real part of the dielectric function, I have investigated the plasmon modes via charge density excitation in the low-temperature and long-wavelength limit.
(6) Using the imaginary part of the inverse dielectric function, I have studied the optical spectrum of a 2DEG via fast electron processes.

In these steps, the effect of the radiation field is included exactly and all possible optical processes, including multiphoton channels, can be included easily. These theoretical approaches are based on time-dependent condensed matter theory on the basis of a non-perturbative treatment for electron interactions with an intense radiation field.

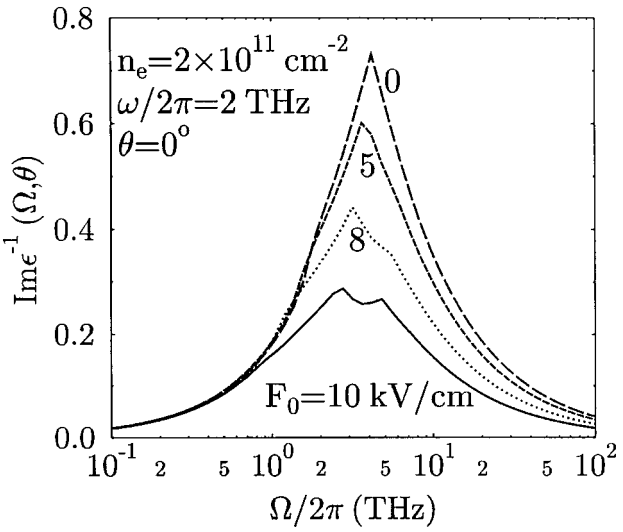

Fig. 7. Influence of the intensity of the driving field F_0 on the optical spectrum at a fixed radiation frequency ω for $\theta = 0^o$. The case $F_0 = 0$ corresponds to the absence of the driving field.

In the presence of a time-dependent driving field such as EM radiation, the electron Green function $G^{\pm}(n, \mathbf{k}; t > t')$, the electron density–density correlation function $\Pi_{n'n}(\mathbf{q}; t, t')$ and the inverse dielectric function matrix element $\epsilon^{-1}_{\alpha\beta}(\mathbf{q}; t, t')$ in the time representation are basically two-time quantities, i.e. they depend

not only on the time relative-coordinates $\tau = t - t'$ but also on the initial time t' or time centre-of-mass $\mathcal{T} = (t + t')/2$. To investigate the steady-state property of a two-time quantity $F(t, t')$ in the presence of an EM field, one approach proposed is (Jauho and Johnsen 1996): (1) Fourier analysing $F(t, t') = F(\tau, \mathcal{T})$ along the τ-direction to get $F(\Omega, \mathcal{T})$, and (2) averaging $\mathcal{T}$ in $F(\Omega, \mathcal{T})$ over a period of the EM field to get $F(\Omega)$ in the spectrum representation. What I have used in the present study in obtaining $F(\Omega)$ from $F(t, t')$ is slightly different from this approach. Here, I first do a Fourier analysis of $F(t, t') = F(\tau, t')$ along the τ-direction to get $F(\Omega, t')$ and then average the initial time t' in $F(\Omega, t')$ over a period of the EM field to obtain $F(\Omega)$. As can be seen from the results obtained in this study, the approach that I have proposed in this paper is more transparent and leads to much simpler analytical results. It can be seen by comparing Fig. 2 of Johnsen and Jauho (1998) with Fig. 2 of the present paper that the two approaches give similar results for a 2DEG driven by an intense laser field. It should be noted that, in sharp contrast to the case where the time-dependent driving field is absent the presence of the EM field will result in a case where the Fourier transform done at different stages may lead to different final results. For example, the only way to calculate correctly the inverse dielectric function matrix element $\epsilon^{-1}_{\alpha\beta}(\mathbf{q}, \Omega)$ in the spectrum representation is to start the calculation directly from $\epsilon^{-1}_{\alpha\beta}(\mathbf{q}; t, t')$ obtained from the RPA diagrams in the time representation. The usage of the RPA diagrams in the spectrum representation with the corresponding pair bubble in the spectrum representation will lead to an incorrect final result for the inverse dielectric function matrix in the spectrum representation.

The theoretical results presented in this paper indicate that the effect of the EM radiation on electronic, optical and optoelectronic properties of an electron gas system can be mainly achieved via two important parameters, $r_0 = eF_0/m^*\omega^2$ with a dimension of length and $\gamma = (eF_0)^2/8m^*\hbar\omega^3$ which is dimensionless. These parameters are connected to the frequency and intensity of the radiation field and to a material parameter such as the effective electron mass of the sample system. For a GaAs-based 2DEG structure subjected to a linearly polarised laser field with frequency $\omega/2\pi \sim 1$ THz and intensity $F_0 \sim 10$ kV cm^{-1}, the conditions such as $r_0 q_x \sim r_0 k_x \sim 1$ and $\gamma \sim 1$ (so $E_{em} = 2\gamma\hbar\omega \sim \hbar\omega$) can be satisfied. As a consequence:

(1) the electron kinetic energy and the Fermi energy of the system are comparable to the THz photon energy and to the radiation field energy induced by the dynamical Franz–Keldysh effect;
(2) the THz radiation will couple strongly to the 2DEG system and will significantly alter the electronic structure of the system;
(3) the momentum and energy relaxation via electronic transitions will be strongly modified by the THz radiation field;
(4) the electronic transition events depend strongly on the change of the electron wavevector along the direction where the radiation field is polarised, which breaks the symmetry of the sample geometry and, consequently, the electronic, optical and optoelectronic properties of a THz-driven 2DEG may become anisotropic; and

(5) as can be seen in this paper, dramatic THz radiation phenomena can be observed theoretically in, for example, electron density of states, Fermi energy, plasmon modes and optical spectrum.

These quantities are experimentally measurable and, most importantly, such radiation conditions have been realised by the THz free-electron laser sources developed recently. It is therefore hoped that the phenomena discussed in this paper will be verified experimentally.

Acknowledgment

This work was supported by the Australian Research Council.

References

Ando, T., Fowler, A. B., and Stern, F. (1982). *Rev. Mod. Phys.* **54**, 437.
Asmar, N. G., Markelz, A. G., Gwinn, E. G., Cerne, J., Sherwin, M. S., Campman, K. L., Hopkins, P. E., and Gossard, A. C. (1995). *Phys. Rev.* B **51**, 18,041.
Asmar, N. G., Cerne, J., Markelz, A. G., Gwinn, E. G., Sherwin, M. S., Campman, K. L., and Gossard, A. C. (1996). *Appl. Phys. Lett.* **68**, 829.
Glicksman, M. (1971). *Solid State Phys.* **26**, 275.
Jauho, A. P., and Johnsen, K. (1996). *Phys. Rev. Lett.* **76**, 4576.
Johnsen, K., and Jauho, A. P. (1998). *Phys. Rev.* B **57**, 8860.
Koenraad, P. M., Lewis, R. A., Waumans, L. R. C., Langerak, C. J. G. M., Xu, W., and Wolter, J. H. (1998). *Physica* B **256–8**, 268.
Markelz, A. G., Asmar, N. G., Brar, B., and Gwinn, E. G. (1996). *Appl. Phys. Lett.* **69**, 3975.
Mattuck, R. D. (1976). 'A Guide to Feynman Diagrams in the Many-body Problem' (McGraw–Hill: New York).
Nordstrom, K. B., Johnsen, K., Allen, S. J., Jauho, A. P., Birnir, B., Kono, J., Noda, T., Akiyama, H., and Sakaki, H. (1998). *Phys. Rev. Lett.* **81**, 457.
Shankar, R. (1980). 'Principles of Quantum Mechanics' (Plenum: New York).
Voβebürger, M., Roskos, H. G., Wolter, F., Waschke, C., Kurz, H., Hirakawa, K., Wilke, I., and Yamanaka, K. (1996). *J. Opt. Soc. Am.* B **13**, 1045.
Xu, W. (1998). *J. Phys.* C **10**, 6105.
Xu, W., and Zhang, C. (1996). *Appl. Phys. Lett.* **68**, 3305.

Manuscript received 19 April, accepted 20 August 1999